Proceedings of the ASME 2016 International Mechanical Engineering Congress & Exposition
IMECE 2016
November 11-17, 2016, Phoenix, Arizona, USA

IMECE2016-65859

VIBRATION ANALYSIS OF A COMPOSITE HELICOPTER ROTOR BLADE AT HOVERING CONDITION

Pratik Sarker
University of New Orleans
New Orleans, LA 70148, USA

Colin R Theodore
NASA Ames Research Center
Mountain View, CA 94035, USA

Uttam K Chakravarty
University of New Orleans
New Orleans, LA 70148, USA

ABSTRACT

The helicopter is an essential and unique means of transport nowadays and needs to hover in space for considerable amount of time. During hovering flight, the rotor blades continuously bend and twist causing an increased vibration level that affects the structural integrity of the rotor blade leading to ultimate blade failure. In order to predict the safe allowable vibration level of the helicopter rotor blade, it is important to properly estimate and monitor the vibration frequencies. Therefore, the mathematical model of a realistic helicopter rotor blade composed of composite material, is developed to estimate the characteristics of free and forced bending-torsion coupled vibration. The cross-sectional properties of the blade are calculated at first and are then included in the governing equations to solve the mathematical model. The natural frequencies and mode shapes of the composite helicopter rotor blade are evaluated for both the nonrotating and rotating cases. The time-varying bending and torsional deflections at the helicopter rotor blade tip are estimated with suitable initial conditions. The validation of the model is carried out by comparing the analytical frequencies with those obtained by the finite element model.

Keywords: Vibration analysis, composite blade, hovering flight, cantilever beam, vertical deflection, finite element.

NOMENCLATURE

A	cross-sectional area
A_d	rotor disk area
B	extensional stiffness of composite shell per unit width
D_b	total bending stiffness of the cross-section
D_t	total torsional stiffness of the cross-section
E	elastic modulus of an isotropic material
E_1	elastic modulus of composite in fiber direction
E_2	elastic modulus of composite in transverse direction
E_{core}	equivalent axial elastic modulus of core
E_{shell}	equivalent axial elastic modulus of composite shell
F_z	external force on the helicopter blade along Z-axis
G_{12}	in plane shear modulus of composite
G_{core}	equivalent shear modulus of core
G_{shell}	equivalent shear modulus of composite shell
I_{NA}	area moment of inertia about the neutral axis
$\bar{I}_p$	area moment of inertia about the principal centroidal axis
$\bar{J}$	polar area moment of inertia about the centroidal axis
M_x	external moment on the helicopter blade about X-axis
V_∞	free stream air velocity
W	normal mode due to bending
W_g	total gross weight of the helicopter
c	chord length of the airfoil
d	distance between neutral axis and centroidal axis
e	distance between the centroid and shear center
f_{nb}	n^{th} natural frequency governed by mainly bending
f_{nt}	n^{th} natural frequency governed by mainly torsion
h_{shell}	thickness of the composite shell
l	length of the helicopter rotor blade
u_p	air velocity normal to the rotor disk plane
u_t	linear blade velocity parallel to the rotor disk plane
w	vertical deflection due to bending along Z-axis
$\bar{y}$	ordinate of any centroid
Φ	normal mode due to torsion
Ω	angular velocity of the rotor blade in rad/s
α_p	pitching angle of the rotor blade
β	blade angle prior to any deformation

γ torsional constant of a section
κ_m polar mass radius of gyration about the elastic axis
$\kappa_{m1,2}$ mass radii of gyration about neutral axis and axis normal to chord through shear center, respectively
θ rotation due to torsion about X-axis
ν Poisson's ratio of an isotropic material
ν_{12} major Poisson's ratio of composite
ρ density of material

INTRODUCTION

Compared to fixed wing aircraft, the helicopter possesses the unique capacity for vertical takeoff and landing, ease of access, hovering for extended periods of time, low speed maneuverability, and flying capability at high altitudes, which has made the helicopter a prolific transport solution with unrivaled versatility. Following this, uses of helicopters cover a variety of military and civil missions, where they need to hover for a significant amount of time by generating the vertical lift force in opposition to its weight which requires the rotor system to be operationally safe and efficient. However, the unsteady aerodynamic loads acting on the helicopter rotor blade and the higher rotational speed of the main rotor, give rise to significant levels of vibration. This vibration, if unnoticed and exceeding a certain level, can reduce the life of the rotor hub by damaging the heavy rotational components. Since it is unlikely to be able to fully eliminate the vibration for a rotary wing aircraft, an estimation of the maximum allowable level of vibration of the helicopter rotor blade is necessary. The frequencies of vibration and the time-varying deflections need to be properly calculated. The airfoil like cross-section of the helicopter rotor blade resembles a rotating cantilever beam having different elastic and inertial axes and, therefore, causes coupling between bending and torsional vibration. Moreover, when the blade is made up of composite material, different ply orientations affect the coupled natural frequencies. Therefore, it is important to investigate the nature of the bending-torsion coupled vibration for a composite helicopter rotor blade in order to identify the effect of the shear center position on the coupled frequencies.

Vibratory loads transferred from the main rotor to the fuselage have been a critical concern from the earliest days of rotorcraft development [1, 2]. Depending on the flight regime, different phenomena become responsible for generating the vibratory loads on the blades. Previous works that showed some investigations on the helicopter hovering performance, varied in the techniques used for analyzing the dynamics based on different assumptions. The first step was to understand the behavior of the aerodynamic environment which created the unbalanced forces acting on the helicopter [3, 4], followed by the derivation of the fundamental equations of motion. For the hovering condition, motion of the helicopter blade is considered as the rotation of a flexible cantilever beam around an axis based on which the free vibration theory is developed [5, 6].

Besides deriving the free vibration equations of motion, rigid body simulations were also carried out. A dynamic model of rotor blades for real-time helicopter simulation was presented which was based on the rigid body simulations, rather than fluid simulation methods [7]. Modeling of the helicopter rotor blade for flapping motion was done by some researchers; however, they considered only the rigid blade which, in reality, is flexible. A general equation describing the helicopter blade dynamics for large flap angle and large induced inflow angle of attack was derived and numerical simulations were performed for steady state conditions [8]. Zaw et al. [9] developed the mathematical model and carried out the stability analysis for an unmanned aerial helicopter using the minimum-complexity helicopter simulation model by MATLAB SIMULINK and considered rigid body dynamics. Numerical techniques were used for the formulation of the equations of motion of general dynamic systems with an emphasis on the equations of motion of helicopter blades [10].

Technical reports were documented after the wind tunnel tests for the helicopter and provided useful information about the pioneering research and specific design database [11–14]. Helicopter blades reported to be tested experimentally are made up of different types of materials. However, instead of metallic blades, composite blades are widely used in modern helicopters due to their high strength to weight ratio [15]. Garinis et al. [16] carried out the modal analysis of the fully composite helicopter blade with honeycomb core to determine the structural mode shapes and natural frequencies. Friedmann et al. [17] developed a moderate deflection composite helicopter rotor blade model with an improved cross-sectional analysis based on the variational asymptotic approach. Among various numerical tools, the finite element (FE) techniques were known as powerful tools to model the rotor blade or a rotating beam for the vibration analysis. Hodges et al. [18] presented the methodologies for predicting the natural frequencies and mode shapes of composite beams with arbitrary cross-sections by FE techniques. Different types of FE methods were examined to verify their efficiencies by finding the frequencies of vibrations [19–21]. In general, most of the FE models contain some basic assumptions to simplify the complex aerodynamic behavior of the helicopter rotor blade.

In most of the previous cases, simulations for rotor blades with different aerodynamic conditions were done considering the blade as a rigid one or FE simulations were done for free vibrations of a blade under pure bending. Therefore, in this paper, the governing equations of bending-torsion coupled vibration of the helicopter rotor blade are developed with a realistic composite rotor blade cross-section to identify the vibration characteristics. The cross-sectional properties of the blade are calculated from the lamination and sandwich beam theory and are included in the one dimensional coupled governing equations of motion. Moreover, the time-varying bending and torsional deflections at the blade tip are estimated by the normal mode method. An FE model of the helicopter rotor blade is created to find the natural frequencies of the coupled vibration for both the nonrotating and rotating cases. The convergence study of the model is checked and validation of the model is done by comparing the analytical natural frequencies with those obtained by the FE analysis.

PROPERTIES OF THE HELICOPTER BLADE

The helicopter rotor blade used in this analysis belongs to the Messerschmitt-Bölkow-Blohm Bo 105 helicopter with the parameters given in Table 1 [13]. From the viewpoint of a realistic helicopter rotor blade, the cross-section is considered to be made up of a thin outer orthotropic fiberglass-epoxy [22] composite shell having the fiber volume fraction as 0.6 and an inner thick isotropic core composed of polymethacrylimide (PMI) foam called Rohacell and honeycomb structures [23, 24] as shown in Fig. 1. The composite shell acts as a balanced laminate built up with four plies with a high strength to weight ratio compared to the inner core and can be considered as a sandwich beam. Properties of the blade materials are given in Tables 2 and 3 [23–25].

TABLE 1: Bo 105 MAIN ROTOR PARAMETERS

Parameters	Value	Parameters	Value
l	4.91 m	Ω	44.5 rad/s
c	0.27 m	Airfoil	NACA 23012

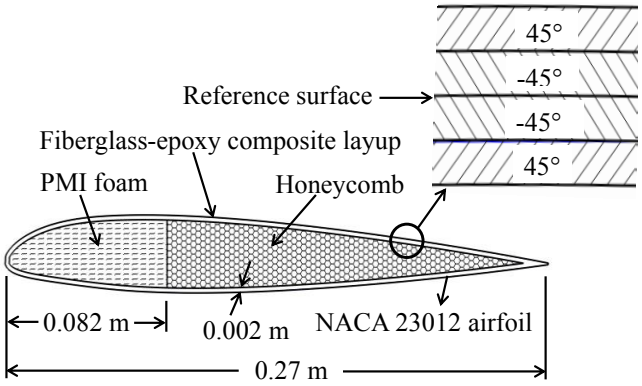

FIGURE 1: CROSS-SECTION OF THE HELICOPTER BLADE

TABLE 2: PROPERTIES OF THE FIBERGLASS-EPOXY COMPOSITE OUTER SHELL

Properties	Value	Properties	Value
ρ	2100 kg/m^3	ν_{12}	0.28
E_1	45e9 Pa	G_{12}	5.5e9 Pa
E_2	12e9 Pa	h_{shell}	0.002 m

TABLE 3: PROPERTIES OF THE ROHACELL-HONEYCOMB ISOTROPIC INNER CORE

Rohacell		Honeycomb	
Properties	Value	Properties	Value
ρ	75 kg/m^3	ρ	48 kg/m^3
E	105e6 Pa	E	128e6 Pa

CROSS-SECTIONAL ANALYSIS OF THE BLADE

Analytical estimation of the cross-sectional properties of the whole composite helicopter rotor blade is difficult to obtain because of the complex geometry and asymmetry of the cross-section described in Fig. 2. However, some reasonable assumptions make the cross-sectional analysis approximate but accurate enough by using the fundamental principles of composite mechanics and classical lamination plate theory. The helicopter rotor blade can be considered as a thin plate so that the plane stress assumptions hold good. However, the curvature effect of the blade section contour must be taken into account. The basic principle of the cross-sectional analysis assumes that the equivalent extensional modulus of elasticity will be the same for the curved composite shell and for a plate laminate made up of the same number of layers, same material, and same length. From that principle, the equivalent extensional modulus of elasticity for the composite shell is estimated and therefore, the extensional stiffness of the shell per unit width is determined. An analytical procedure is developed to find the bending stiffness of the cross-section using the extensional stiffness per unit width [26]. To apply this theory, the equation of the reference surface profile of the shell is necessary. To determine the equation of the reference curve which is the middle surface of the shell, a curve fitting operation is carried out in MATLAB. At first, the outermost shell profile in Fig. 1 is generated from the NACA 23012 data [27] and then the reference curve data set is generated from the former having an offset distance of 0.001 m using differential calculus slope theory. Next, these data points are centered and fitted in MATLAB to get an approximate equation in the form of a 10th degree polynomial. This theory is applied to find the natural frequencies of free vibration of a thin circular composite shell composed of four layers [18] and good agreement is found between the natural frequencies obtained from the theory and from Ref. 18. The geometric sectional properties are calculated from the commercially available computer aided design package SolidWorks 2015.

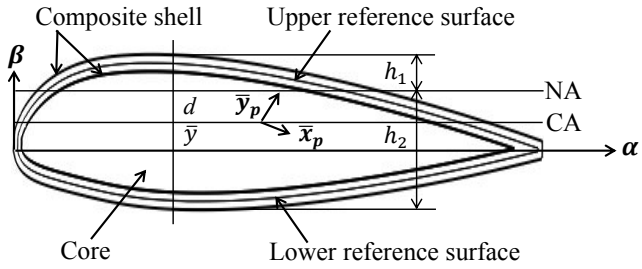

FIGURE 2: LOCATION OF THE CA and NA OF THE BLADE

In Fig. 2, the α and β axes are the coordinate axes of the outermost profile of the blade cross-section. From Fig. 2, the centroidal axis (CA) and the principal centroidal $\bar{x}_p$-axis are not exactly aligned. However, the separation angle is approximately 1° and is negligibly small to affect the section properties of both the shell and the core. The bending stiffness

of the whole cross-section is to be calculated with respect to the neutral axis (NA) of the section which is not located at the geometric centroid of the cross-section. The geometric properties of the cross-section are: $\bar{y}_{shell}$ = 2.86e-3 m, $\bar{y}_{core}$ = 3.57e-3 m, A_{shell} = 1.06e-3 m^2, A_r = 8.97e-4 m^2, A_h = 4.03e-3 m^2, $\bar{I}_{p_{shell}}$ = 1.33e-7 m^4, $\bar{I}_{p_{core}}$ = 2.27e-7 m^4, γ_{shell} = 3.869e-7 m^4, γ_{core} = 7.839e-7 m^4, and e = 0.009 m, where r and h stand for the Rohacell and honeycomb structures, respectively.

Extensional Stiffness Per Unit Width

From lamination theory [28],

$$E_{shell} = \frac{A_{11}A_{22} - A_{12}^2}{h_{shell}A_{22}}. \quad (1)$$

where, A_{11}, A_{12}, and A_{22} are the elements of the extensional stiffness matrix of a composite laminate. Then B is evaluated as,

$$B = \frac{E_{shell}A_{shell}}{s_{uref} + s_{lref}}. \quad (2)$$

where, s_{uref} and s_{lref} are the arc lengths of the upper and the lower reference curves, respectively, shown in Fig. 2.

Bending Stiffness

Using the value of B and including the curvature effect of the cross-sectional profile, bending stiffness of the composite shell is estimated as [26],

$$E_{shell}\bar{I}_{pshell} = B\left[\int_{0.001}^{0.2651} y_{uref}^2 ds + \int_{0.001}^{0.2651} y_{lref}^2 ds\right]. \quad (3)$$

where, y_{uref} and y_{lref} are the ordinates of the upper and lower reference curves obtained from MATLAB curve fitting. Equation (4) provides a reasonable modulus for the core when the constituent materials have relatively close E values.

$$E_{core} = \frac{E_rA_r + E_hA_h}{A_r + A_h}. \quad (4)$$

where, r and h stands for the Rohacell and honeycomb structures. Considering linear strain distribution, location of the NA for the whole cross-section is found from Eqs. (6) and (7).

$$E_{shell}d_{shell}A_{shell} + E_{core}d_{core}A_{core} = 0. \quad (5)$$

$$\Rightarrow E_{shell}(y_{upper} - h_1 - \bar{y}_{shell})A_{shell} + E_{core}(y_{upper} - h_1 - \bar{y}_{core})A_{core} = 0. \quad (6)$$

$$h_1 + h_2 = 0.03. \quad (7)$$

In Eq. (6), y_{upper} = 0.0183 m and y_{lower} = − 0.0117 m, defined as the ordinates of the topmost and bottommost surfaces, respectively, at α = 0.123 m, which is the location of the centroid of the whole section. D_b is calculated from Eq. (10) using Eqs. (8) and (9).

$$I_{NA_{shell}} = \bar{I}_{p_{shell}} + A_{shell}d_{shell}^2. \quad (8)$$

$$I_{NA_{core}} = \bar{I}_{p_{core}} + A_{core}d_{core}^2. \quad (9)$$

$$D_b = E_{shell}I_{NA_{shell}} + E_{core}I_{NA_{core}}. \quad (10)$$

Torsional Stiffness

The estimate of the individual shear modulus for the shell and the core can be approximated as [28],

$$G_{shell} = \frac{A_{66}}{h_{shell}}. \quad (11)$$

$$G_{core} = \frac{E_{core}}{2(1+\nu)}. \quad (12)$$

where, A_{66} is the element of the extensional stiffness matrix of a composite laminate. Equation (12) is an approximate validation since both the Rohacell foam and honeycomb structures are isotropic and use the same ν. The shear center and centroid of the cross-section are relatively close to each other and the total torsional stiffness is written as,

$$D_t = G_{shell}\gamma_{comp} + G_{core}\gamma_{core}. \quad (13)$$

Mass Per Unit Length

The mass per unit length of the rotor blade section is the sum of the masses per unit length of all the constituent materials expressed as,

$$\rho A = \sum_{i=1}^{3}(\rho A)_i. \quad (14)$$

$$\Rightarrow \rho A = \rho_{shell}A_{shell} + \rho_rA_r + \rho_hA_h. \quad (15)$$

ANALYTICAL FORMULATION

Free Vibration

The helicopter rotor blade element considered for the bending-torsion coupled vibration analysis is described in Fig. 3. To derive the coupled equations of motion, the blade cross-section needs to have at least one axis of symmetry which is not the case for the proposed blade cross-section. This situation is overcome by the fact that the principal centroidal $\bar{x}_p$-axis is at an angle of only 1° with the horizontal CA (Fig. 2), not large enough to affect the inertia properties. Therefore, the blade can be considered symmetric with respect to the principal centroidal $\bar{x}_p$-axis, where e is considered a horizontal distance. The effect of the cross-sectional warping is ignored for its relatively minor role for solid sections [20]. The equations of motion of the coupled bending-torsion vibration of the rotor

blade for the nonrotating and rotating cases with zero external force and moment per unit length, $F_z/l(x,t)$ and $M_x/l(x,t)$, respectively, are given by Eqs. (16)–(19) [29–30]. The axial tensile force developed due to the centrifugal action is assumed to pass through the geometric centroid of the cross-section.

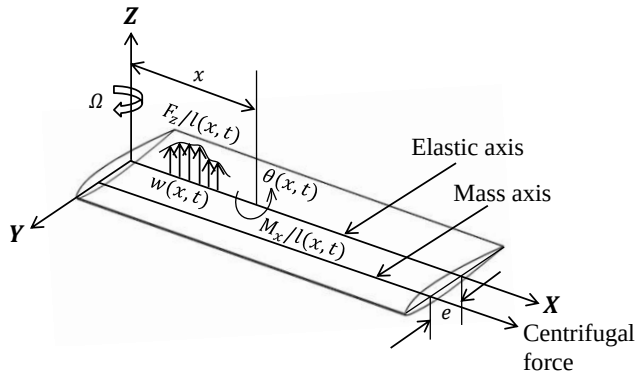

FIGURE 3: THE ROTOR BLADE ELEMENT SUBJECTED TO BENDING AND TORSIONAL DEFORMATIONS

Equations of Motion: Nonrotating Case

$$D_b\frac{\partial^4 w(x,t)}{\partial x^4}+\rho A\left[\frac{\partial^2 w(x,t)}{\partial t^2}-e\frac{\partial^2\theta(x,t)}{\partial t^2}\right]=0. \quad (16)$$

$$D_t\frac{\partial^2\theta(x,t)}{\partial x^2}+\rho A\left[e\frac{\partial^2 w(x,t)}{\partial t^2}-e^2\frac{\partial^2\theta(x,t)}{\partial t^2}\right]-\rho\bar{J}\frac{\partial^2\theta(x,t)}{\partial t^2}=0. \quad (17)$$

Equations of Motion: Rotating Case

$$\begin{aligned}D_b\frac{\partial^4 w(x,t)}{\partial x^4}&-\frac{\partial}{\partial x}\left(T(x)\frac{\partial w(x,t)}{\partial x}\right)\\&-\rho Ae\Omega^2\cos\beta\left[\theta+x\frac{\partial\theta(x,t)}{\partial x}\right]\\&+\rho A\left[\frac{\partial^2 w(x,t)}{\partial t^2}+e\frac{\partial^2\theta(x,t)}{\partial t^2}\cos\beta\right]\\&=0.\end{aligned} \quad (18)$$

$$\begin{aligned}-D_t\frac{\partial^2\theta(x,t)}{\partial x^2}&+\rho Ae\Omega^2 x\frac{\partial w(x,t)}{\partial x}\cos\beta\\&+\rho A\Omega^2[\kappa_{m2}^2-\kappa_{m1}^2]\theta(x,t)\cos(2\beta)\\&+\rho A\kappa_m^2\frac{\partial^2\theta(x,t)}{\partial t^2}+\rho Ae\frac{\partial^2 w(x,t)}{\partial t^2}\cos\beta\\&=0.\end{aligned} \quad (19)$$

where,

$$T(x)=\int_x^l \rho A\Omega^2 x dx. \quad (20)$$

Forced Vibration: Aerodynamic Force and Moment

When the helicopter maintains its hovering flight, the total lift produced by the rotor blades must be at least equal to the W_g. This amount of lift can be calculated from the blade element theory (BET) [3]. From the assumption of low disk loading, the inflow ratio is considered to be as small as 0.06. Then, the ratio of the u_p and u_t also becomes small and this small angle assumption is applicable for the inflow angle, the pitching angle, and the angle of attack. For the hovering flight with no axial velocity, the induced velocity becomes equal to u_p. Also, it is assumed that the stall and the compressibility effects are negligible so that the lift coefficient is linearly related to the angle of attack. There is always some free stream velocity at any altitude which is also considered to find the lift equation using the BET. Finally, the aerodynamic lift and moment per unit length for a single blade are given by,

$$\frac{F_z|_{BET}}{l}(x,t)=\frac{1}{2}\rho_{air}u_t^2 ca\left(\alpha_p-\frac{u_p}{u_t}\right). \quad (21)$$

$$\frac{M_x}{l}(x,t)=0.0555\frac{F_z|_{BET}}{l}(x,t). \quad (22)$$

where,

$$u_t=[\Omega x+V_\infty sin(\Omega t)]. \quad (23)$$

$$u_p=\sqrt{W_g/2\rho_{air}A_d}. \quad (24)$$

with a = 5.7, ρ_{air} = 1.225 kg/m^3, V_∞ = 0.5 m/s, W_g = 24525 N, and A_d = 76 m^2. It is conventional to consider that $F_z|_{BET}/l$ passes through the aerodynamic center which is 1/4 of the chord from the leading edge. M_x/l is the moment of $F_z|_{BET}/l$ about the mass center of the blade cross-section, since, the shear center and the mass center of the cross-section are very close. For a specific value of Ω, if α_p is much greater, then $F_z|_{BET}$ for a single blade can exceed the total lift force estimated from the disk loading (DL), where, $DL=W_g/A_d$. Therefore, an optimization is made between Ω and α_p, unless the following relationship for a single blade is satisfied,

$$F_z|_{BET}\approx F_z|_{DL}. \quad (25)$$

Equations of Motion: Forced Vibration

For a single blade, $F_z|_{DL}=(DL)cl=428$ N. Using Eq. (25), for Ω = 44.5 rad/s, α_p is found to be 0.5° and the forced vibration equations with $\beta=\alpha_p$ take the form as mentioned below:

$$\begin{aligned}D_b\frac{\partial^4 w(x,t)}{\partial x^4}&-\frac{\partial}{\partial x}\left(T(x)\frac{\partial w(x,t)}{\partial x}\right)\\&-\rho Ae\Omega^2\cos\alpha_p\left[\theta+x\frac{\partial\theta(x,t)}{\partial x}\right]\\&+\rho A\left[\frac{\partial^2 w(x,t)}{\partial t^2}+e\frac{\partial^2\theta(x,t)}{\partial t^2}\cos\alpha_p\right]\\&=\frac{F_z|_{BET}}{l}(x,t).\end{aligned} \quad (26)$$

$$-D_t\frac{\partial^2\theta(x,t)}{\partial x^2}+\rho Ae\Omega^2 x\frac{\partial w(x,t)}{\partial x}cos\alpha_p + \rho A\Omega^2[\kappa_{m2}^2-\kappa_{m1}^2]\theta(x,t)\,cos(2\alpha_p) + \rho A\kappa_m^2\frac{\partial^2\theta(x,t)}{\partial t^2}+\rho Ae\frac{\partial^2 w(x,t)}{\partial t^2}cos\alpha_p = \frac{M_x}{l}(x,t). \quad (27)$$

Boundary Conditions

Solutions of the boundary value problems in Eqs. (16)–(19) and Eqs. (26)–(27) must satisfy the relevant boundary conditions specified as,

$$at\ x=0:\quad w(0,t)=0.;\ \frac{dw(0,t)}{dx}=0.;\ \theta(0,t)=0. \quad (28)$$

$$at\ x=l:\ \frac{d^2w(l,t)}{dx^2}=0.;\ \frac{d^3w(l,t)}{dx^3}=0.;\ \frac{d\theta(l,t)}{dx}=0. \quad (29)$$

Initial Conditions

The initial conditions for Eqs. (26)–(27) are determined using linear deflection and angular deformation assumptions and are stated as,

$$w(x,0)=0.0175x.;\qquad \frac{\partial w}{\partial t}(x,t)=0. \quad (30)$$

$$\theta(x,0)=0.005332x.;\qquad \frac{\partial\theta}{\partial t}(x,t)=0. \quad (31)$$

Solution Strategy: Free Vibration-Nonrotating Case

Solutions of Eqs. (16)–(17), after satisfying Eqs. (28)–(29) assume the forms,

$$w(x,t)=W(x)C_1\cos(\omega t+\theta_1). \quad (32)$$

$$\theta(x,t)=\Phi(x)C_2\cos(\omega t+\theta_2). \quad (33)$$

where,

$$W(x)=a_n[\cosh(\beta_n x)-\cos(\beta_n x) - \sigma_n[\sinh(\beta_n x)-\sin(\beta_n x)]\,] = a_n F(x). \quad (34)$$

$$\Phi(x)=b_n\sin\left[\frac{(2n-1)\pi x}{2l}\right]=b_n H(x). \quad (35)$$

$$\sigma_n=\frac{\sinh(\beta_n l)-\sin(\beta_n l)}{\cosh(\beta_n l)+\cos(\beta_n l)}. \quad (36)$$

with a_n and b_n as arbitrary constants, $\beta_n l$ as the root of the characteristic equation of transverse vibration of a cantilever beam [29], and ω as the natural frequency in rad/s.

Using Eqs. (32)–(33) into Eqs. (16)–(17) with $C_1=C_2$ and $\theta_1=\theta_2$,

$$D_b W''''(x)=\rho A\omega^2[W(x)-e\Phi(x)]. \quad (37)$$

$$D_t\Phi''(x)=\rho A\omega^2 e[W(x)-e\Phi(x)]-\rho\bar{J}\omega^2\Phi(x). \quad (38)$$

Substituting Eqs. (34)–(35) into Eqs. (37)–(38),

$$[D_b\beta_n^4F(x)-\rho A\omega_n^2F(x)]a_n+\rho A\omega_n^2eH(x)b_n=0. \quad (39)$$

$$\rho A\omega_n^2eF(x)a_n+[D_tQ_nH(x)-\rho A\omega_n^2e^2H(x)-\rho\bar{J}\omega_n^2H(x)]b_n=0. \quad (40)$$

where,

$$Q_n=(2n-1)^2\pi^2/4l^2. \quad (41)$$

Solution of Eqs. (39)–(40) requires the determinant of the coefficients of a_n and b_n to be vanished as,

$$\begin{vmatrix}(D_b\beta_n^4-\rho A\omega_n^2)F(x) & \rho A\omega_n^2eH(x)\\ \rho A\omega_n^2eF(x) & (D_tQ_n-\rho A\omega_n^2e^2-\rho\bar{J}\omega_n^2)H(x)\end{vmatrix}=0. \quad (42)$$

from which,

$$f_{nb}=\frac{1}{2\pi}\sqrt{\frac{u^2-\sqrt{(u^2)^2-4v^2}}{2k^2}}. \quad (43)$$

and,

$$f_{nt}=\frac{1}{2\pi}\sqrt{\frac{u^2+\sqrt{(u^2)^2-4v^2}}{2k^2}}. \quad (44)$$

where, $p^2=Q_n$, $u^2=p^2q^2+g^2e^2\beta_n^4+k^2g^2\beta_n^4$, $v^2=k^2g^2\beta_n^4p^2q^2$, $q^2=D_t/\rho A$, $g^2=D_b/\rho A$, $k^2=\bar{J}/A$, and $A=A_{shell}+A_{core}$, with $A_{core}=A_r+A_h$.

Solution Strategy: Free Vibration-Rotating Case

For the rotating slender blade, the rotational stiffness becomes much higher than the normal bending stiffness and affects f_{nb} significantly leaving f_{nt} almost unaffected. Moreover, e in Eqs. (18) and (19) is small enough compared to c for which the term $g^2e^2\beta_n^4$ becomes negligible to maintain a significant coupling between bending and torsion. These two assumptions suggest that, the uncoupled bending vibration solution strategy can offer very good results as a substitute for the coupled vibration solution. However, use of this method requires the mode shape of the rotating blade [6] due to uncoupled bending vibration. When this is included, Eqs. (18) and (19) are considered to be weakly coupled and f_{nb} is approximated as,

$$f_{nb}=\frac{1}{2\pi}\sqrt{\frac{D_b}{\rho Al^4}\frac{\alpha_1}{\alpha_3}+0.5\Omega^2\frac{\alpha_2}{\alpha_3}}. \quad (45)$$

where, values of α_1, α_2, and α_3 are listed in Table 4 for the first three modes. Unlike f_{nb}, f_{nt} would not be influenced significantly by the rotational stiffness and is increased only by a slight amount. This is evident in the results and discussions section.

TABLE 4: VALUES OF α_1, α_2, AND α_3 FOR THE FIRST THREE BENDING MODES OF A ROTATING BLADE

n	$\beta_n l$	α_1	α_2	α_3
1	1.875	22.95	4.43	1.86
2	4.694	468.04	12.49	0.964
3	7.855	3812.81	35.78	1.00

Solution Strategy: Forced Vibration

The solution of the forced vibration in Eqs. (26)–(27) is approximated from the normal mode method as,

$$w(x,t) = \sum_{n=1}^{\infty} \xi_n(t) W_{nr}(x). \quad (46)$$

$$\theta(x,t) = \sum_{n=1}^{\infty} \xi_n(t) \Phi_n(x). \quad (47)$$

where, ξ_n is the generalized time coordinate for the n^{th} mode and W_{nr} is the rotating blade mode shape [6] with,

$$\xi_n(t) = A_n \cos(\omega_n t) + B_n \sin(\omega_n t) + \frac{1}{\rho A \omega_n} \int_0^t P_n(\tau) \sin[\omega_n (t-\tau)]\, d\tau. \quad (48)$$

and,

$$P_n(\tau) = \int_0^l \left[\frac{F_z|_{BET}}{l}(x,\tau) W_{nr}(x) + \frac{M_x}{l}(x,\tau) \Phi_n(x) \right] dx. \quad (49)$$

The following orthogonality relationships are used to find the values of the contants a_n and b_n.

$$\int_0^l W_{nr}^2(x)dx = 1.; \qquad \int_0^l \Phi_n^2(x)dx = 1. \quad (50)$$

FINITE ELEMENT ANALYSIS

The FE model of the helicopter rotor blade is created using the commercially available FE package, Abaqus 6.12. The whole rotor blade is modeled as a cantilever beam composed of two parts: the outer composite shell and the inner isotropic core. Both the inner surface of the shell and the outer surface of the core are assigned tie constraints so that they act together as a whole body. Both the composite shell and the core of the blade are meshed with the finest element size of 0.008 m. After meshing, the shell has 41,752 elements and 41,820 nodes and the core has 77,978 elements and 99,630 nodes. For meshing the composite shell, S4R (four-node doubly curved thin or thick shell) elements are used and for the core, C3D8R (eight-node, linear brick, reduced integration) elements are used.

RESULTS AND DISCUSSIONS

Convergence Study

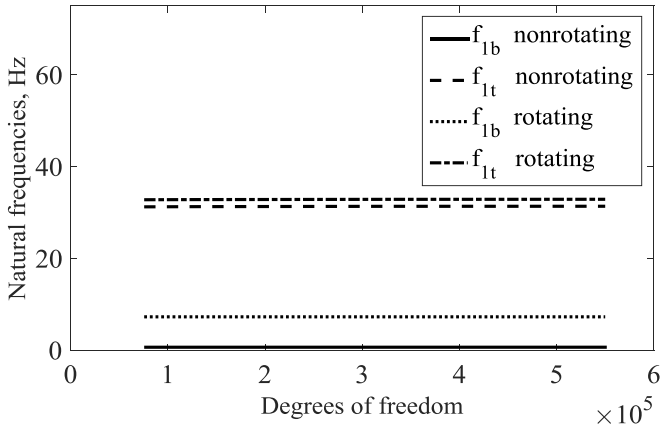

FIGURE 4: VARIATION OF THE FUNDAMENTAL NATURAL FREQUENCIES OF THE COUPLED VIBRATION WITH DEGREES OF FREEDOM

Figure 4 explains the variation of the fundamental natural frequencies of the bending-torsion coupled vibration with the degrees of freedom (DOF) for nonrotating and rotating cases. From Fig. 4, as the DOF increases, the trends of the natural frequencies become flattened after showing some initial change indicating that the solution is already converged. For both the nonrotating and the rotating cases, same mesh densities for both the shell and the core are used with the finest element size of 0.008 m.

Frequencies and Mode Shapes: Nonrotating Case

Table 5 lists the natural frequencies of the free bending-torsion coupled vibration of the nonrotating helicopter rotor blade for the first three modes by the analytical and the FE method. Here, f_{nb}(n = 1, 2, 3…) is for a mode where the deformation is mainly due to bending and torsion plays a minor role. Similarly, f_{nt} is for a mode where torsion causes the major deformation rather than bending. Table 5 shows reasonable agreement between the analytical and the FE results substantiating a good validation of the analytical method used to calculate the cross-sectional properties. The error level of f_{nb} is lower than that of f_{nt} indicating that the analytical estimate of D_t is a little higher than that from the FE method. However, f_{nt} is less sensitive to error than f_{nb} and one reason for this is, for a particular mode, f_{nt} is much higher in magnitude than f_{nb}. Another explanation is that, the blade can be considered as a long thin plate due to its geometry which is more prone to bending rather than torsion. The effect of e on the bending-torsion coupling is small as predicted before since the shear

center is very close to the centroid. This is justified by the first free uncoupled bending vibration frequency as $\left[(1.875/l)^2\sqrt{D_b/\rho A}\right]/2\pi$ = 0.69 Hz which is the same as f_{1b}. However, in higher modes, the coupling effect can be influencial with relatively greater effect of e on the natural frequencies which explains the decreasing error of f_{nt} for higher modes in Table 5.

TABLE 5: NATURAL FREQUENCIES OF THE COUPLED VIBRATION FOR THE NONROTATING BLADE

	Natural frequencies, Hz		% Error
	Analytical	FE	
f_{1b}	0.69	0.65	5.79
f_{1t}	35.64	31.36	12
f_{2b}	4.33	4.04	6.69
f_{2t}	106.92	93.93	12.12
f_{3b}	12.13	11.27	7.09
f_{3t}	178	157.10	11.74

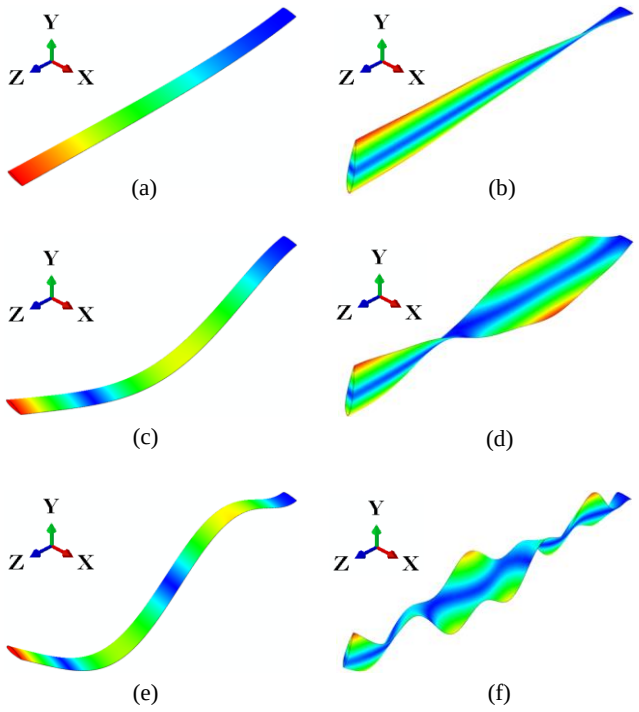

FIGURE 5: MODE SHAPES OF THE NONROTATING BLADE GOVERNED BY (a) 1st MODE BENDING (b) 1st MODE TORSION (c) 2nd MODE BENDING (d) 2nd MODE TORSION (e) 3rd MODE BENDING (f) 3rd MODE TORSION

Figures 5(a) through 5(f) depict the mode shapes of the coupled bending-torsion vibration of the nonrotating helicopter rotor blade. The fundamental bending governed mode shape is given in Fig. 5(a) with no node along the length of the blade while Fig. 5(b) shows the fundamental torsion governed mode having a blue axis running parallel to the elastic axis of the blade. This axis goes through the shear center suggesting that the blade is about to rotate with respect to this axis. Figures 5(c) and 5(d) explain the similar phenomena for the second mode governed by bending and torsion, respectively, each having one node. Following this, Figs. 5(e) and 5(f) describe the third mode governed by bending and torsion, respectively, having two nodes each. Although, the coupling effect as seen from the mode shapes seems to be smaller, it can gradually become larger with higher modes as previously discussed. This seems possible from Fig. 5(f), where the blue axis gets distorted due to the coupled bending effect. From the first three mode shapes in Fig. 5, the blade can be considered to vibrate close to its fundamental modes.

Frequencies and Mode Shapes: Rotating Case

TABLE 6: NATURAL BENDING GOVERNED FREQUENCIES OF THE COUPLED VIBRATION FOR THE ROTATING BLADE

	Natural frequencies, Hz		% Error
	Analytical	FE	
f_{1b}	7.77	7.27	6.43
f_{2b}	18.54	18.06	2.59
f_{3b}	32.30	30.17	6.59

TABLE 7: NATURAL TORSION GOVERNED FREQUENCIES OF THE COUPLED VIBRATION FOR THE ROTATING BLADE

	Natural frequencies, Hz		% Increase
	Nonrotating case	Rotating case	
f_{1t}	31.36	32.88	4.84
f_{2t}	93.93	95.45	1.61
f_{3t}	157.10	161.02	2.49

As compared to f_{nb} results from Table 5 for the nonrotating case, Table 6 lists the first three f_{nb} results for the rotating case. This time, the f_{nb} is much higher than the f_{nb} for the nonrotating case. This is due to the addition of the rotational stiffness developed by the rotating blade for which the contribution is significantly greater than the nonrotating f_{nb}. The high rotational stiffness weakens the coupling between bending and torsion and significantly affects the bending behavior, rather than torsion. Based on this fact, the solution methodology for the uncoupled bending vibration is proposed in place of the solution of the coupled case and the justification is seen from Table 6 where the frequencies obtained by the analytical and the FE method are in good agreement with the maximum error of 6.59%. The rotational stiffness also adds to the f_{nt}, however, with much less priority compared to the f_{nb}. Table 7 shows a comparison of the f_{nt} obtained from the FE analysis for the nonrotating and rotating cases where, f_{1t} increases by 4.84% for the rotating case. On the other hand, from Tables 5 and 6, f_{1b} increases by 1018% showing the more severe influence of the rotational stiffness on f_{nb}.

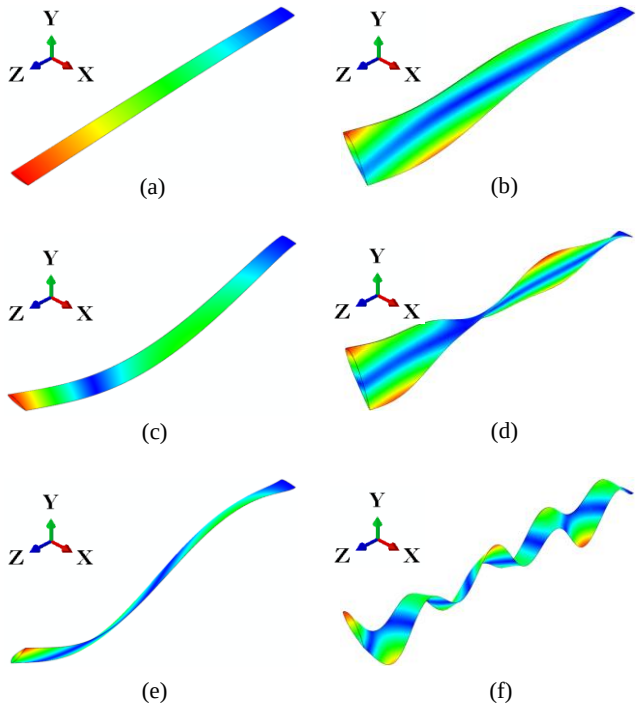

FIGURE 6: MODE SHAPES OF THE ROTATING BLADE GOVERNED BY (a) 1st MODE BENDING (b) 1st MODE TORSION (c) 2nd MODE BENDING (d) 2nd MODE TORSION (e) 3rd MODE BENDING (f) 3rd MODE TORSION

Figures 6(a) through 6(f) describe the mode shapes of the coupled bending-torsion vibration of the rotating helicopter blade. These mode shapes are similar to that of Fig. 5; however, unlike Fig. 5, they are affected by the additional rotational stiffness which makes them more taut. The effect is, as usual, more significant for the bending governed modes than the torsion governed ones. The torsion governed mode shapes in Figs. 6(b), 6(d), and 6(f) show that they do not maintain the exact sinusoidal pattern as used in the nonrotating coupled vibration. This is also true for the bending governed modes, where the mode shape used, is that for the rotating blade.

Time-Varying Deflections: Forced Vibration

Figures 7 and 8 explain the characteristics of the time-varying bending and torsional deflections, respectively, at the helicopter rotor blade tip ($x/l = 1$), showing that both of them are harmonic in nature. From Fig. 7, the deflection starts from 0.086 m and fluctuates between 0.119 and 0.01 m, all of which are positive. This is due to the positive magnitude of the forcing function for all the time. Starting from the initial deflected position, the tip is subjected to more downward deflection than upward and after that, finds its own equilibrium position. From Fig. 8, the torsional deflection starts from 0.026 rad and fluctuates between the maximum and minimum values of 0.025 rad and -0.02 rad, respectively. Unlike the bending case, the torsional deflection goes through both positive and negative values from equilibrium position. This is attributable to the magnitude of the moment function which is small enough to create positive deflection all the time. The frequency of the deflection for bending is much less than that of the torsion.

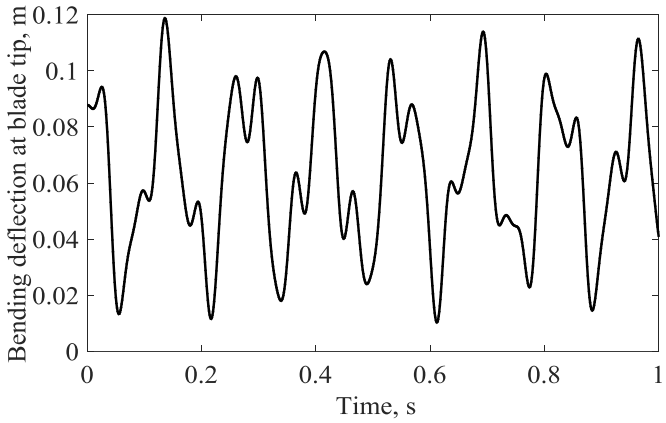

FIGURE 7: TIME-VARYING BENDING DEFLECTION AT THE TIP OF THE HELICOPTER ROTOR BLADE

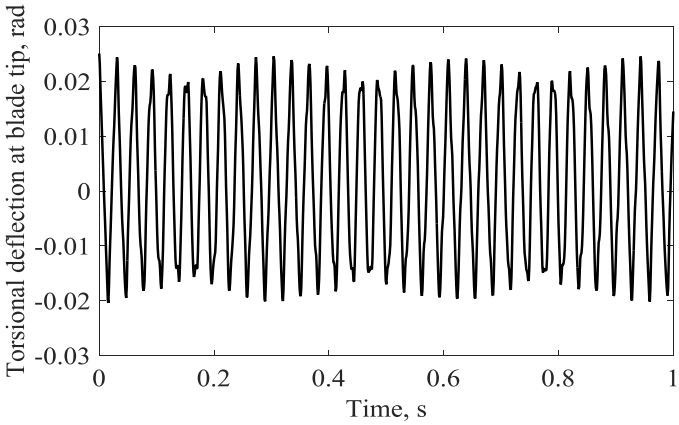

FIGURE 8: TIME-VARYING TORSIONAL DEFLECTION AT THE TIP OF THE HELICOPTER ROTOR BLADE

CONCLUSIONS

In this paper, the coupled free and forced bending-torsion vibration analysis of a composite helicopter rotor blade is carried out for hovering condition in terms of the natural frequencies and time-varying bending and torsional deflections by analytical and finite element methods. The following conclusions are drawn from the analysis:

1. The nonrotating case frequencies are less than the rotating case frequencies for both bending and torsion governed modes. This is due to the additional stiffness developed by the centrifugal force which significantly affects the bending governed modes more than the torsion governed modes.

2. The effect of the coupling between bending and torsion is not that large due to the relative closeness of the locations of the mass center and the shear center of the blade cross-section.

3. The error between the analytical and the finite element torsion governed frequencies for the nonrotating case

are higher compared to that of the bending governed ones. This is due to relatively less accurate estimation of the torsional stiffness than the bending stiffness which is compensated by the additional rotational stiffness developed by the rotating blade.

4. The effectiveness of the solution strategy for the coupled bending-torsion vibration for a rotating blade depends on the strength of coupling, the slenderness of the blade, and the magnitude of the rotational stiffness. For a slender blade with relatively high rotational stiffness and a closer shear center relative to the mass center, the uncoupled vibration solution strategy offers a reasonably accurate approximate solution.

5. The time-varying bending and torsional deflections are both harmonic in nature and the frequency of torsional deflection is greater than that of the bending deflection. The torsional deflection changes from positive to negative peaks unlike the bending case because of lower order of magnitude of the moment load compared to that of the initial condition.

REFERENCES

[1] Gerstenberger, W., Wagner, R. A., Kelley, B., and Ellis, C. W., 1957, "The Rotary Round Table: How Can Helicopter Vibrations be Minimized," J. of the American Helicopter Society, **2**(3).

[2] Loewy, R. G., 1980, "Helicopter Vibrations: A Technological Perspective," J. of the American Helicopter Society, **29**(4).

[3] Johnson, W., 1994, *Helicopter Theory*, Dover Publications.

[4] Leishman, J. G., 2006, *Principles of Helicopter Aerodynamics*, Cambridge University Press.

[5] Bramwell, A. R. S., Done, G., and Balmford, D., 2001, *Bramwell's Helicopter Dynamics*, American Institute of Aeronautics and Astronautics.

[6] Genta, G., 2005, *Dynamics of Rotating Systems*, Springer.

[7] Park, S., Baek, N., and Ryu, K., 2012, "A Dynamics Model of Rotor Blades for Real-Time Helicopter Simulation," Int. J. of Multimedia and Ubiquitous Engineering, **7**(2), pp. 209–220.

[8] Majhi, J. R., and Ganguli, R., 2008, "Modeling Helicopter Rotor Blade Flapping Motion Considering Nonlinear Aerodynamics," Computer Modeling in Engineering and Sciences, **27**(1), pp. 25–36.

[9] Zaw, M. T., Tun, H. M., and Naing, Z. M., 2014, "Development of Mathematical Model and Stability Analysis for UAH," Int. J. of Scientific and Research Publications, **4**(5).

[10] Rand, O., and Barkai, S. M., 1995, "Numerical Evaluation of the Equations of Motion of Helicopter Blades with Symbolic Exactness," J. of the American Helicopter Society, **40**(1), pp. 59–71.

[11] Shinoda, P. M., 2004, "Investigation of a Full-Scale Wide Chord Blade Rotor System in the NASA Ames 40- by 80-Foot Wind Tunnel," *American Helicopter Society, 4th Decennial Specialist's Conference on Aeromechanics*, California.

[12] Bousman, W. G., 2003, "Aerodynamic Characteristics of SC1095 and SC1094 R8 Airfoils," NASA Technical Paper 212265, Ames Research Center, California.

[13] Peterson, R. L., 1995, "Full-Scale Hingeless Rotor Performance and Loads," NASA Technical Memorandum 110356, Ames Research Center, California.

[14] Brooks, T. F., Jolly, Jr., J. R., and Marcolini, M. A., 1988, "Helicopter Main-Rotor Noise: Determination of Source Contributions Using Scaled Model Data," NASA Technical Paper 2825, Virginia.

[15] Hopkins, S. A., and Ormiston, R. A., 2003, "An Examination of Selected Problems in Rotor Blade Structural Mechanics and Dynamics," *American Helicopter Society, 59th Annual Forum*, Phoenix, Arizona.

[16] Garinis, D., Dinulović, M., and Rašuo, B., 2012, "Dynamic Analysis of Modified Composite Helicopter Blade," *Faculty of Mechanical Engineering Transactions*, **40**(2), pp. 63–68.

[17] Friedmann, P. P., Glaz, B., and Palacios, R., 2009, "A Moderate Deflection Composite Helicopter Rotor Blade Model with Improved Cross-Sectional Analysis," International J. of Solids and Structures, **46**, pp. 2186–2200.

[18] Hodges, D. H., Atilgan, A. R., Fulton, M. V., and Rehfield, L. W., 1991, "Free-Vibration Analysis of Composite Beams," J. of American Helicopter Society, **36**(3), pp. 36–47.

[19] Banerjee, J. R., and Williams, F. W., 1994, "Coupled Bending-Torsional Dynamic Stiffness Matrix of an Axially Loaded Timoshenko Beam Element," International J. of Solids and Structures, **31**(6), pp. 749–762.

[20] Hashemi, S. M., and Richard, M. J., 2000, "Free Vibrational Analysis of Axially Loaded Bending-Torsion Coupled Beams: A Dynamic Finite Element," Computers and Structures, **77**(6), pp. 711–724.

[21] Kaya, M. O., and Ozgumus, O. O., 2007, "Flexural-Torsional-Coupled Vibration Analysis of Axially Loaded Closed-Section Composite Timoshenko Beam by Using DTM," J. of Sound and Vibration, **306**, pp. 495–506.

[22] Salkind, M., and Hollister, G., 1973, *Applications of Composite Materials*, STP 524, ASTM, Philadelphia.

[23] Product Information-Rohacell RIST, Evonik Industries, Essen, Germany.

[24] HexWeb Honeycomb Attributes and Properties, Hexcel Corporation, Stamford, Connecticut.

[25] Rasheed, H. A., 2014, *Strengthening Design of Reinforced Concrete with* FRP, Taylor & Francis/CRC Press.

[26] Vasiliev, V. V., and Morozov, E. V., 2013, *Advanced Mechanics of Composite Materials and Structural Elements*, Elsevier.

[27] Airfoil Coordinates Database, UIUC Applied Aerodynamics Group, Urbana, Illinois.

[28] Yu, A. M., Yang, J. W., Nie, G. H., and Yang, X. G., 2011, "An Improved Model for Naturally Curved and Twisted Composite Beams," Composite Structures, **93**, pp. 2322–2329**.**

[29] Weaver, Jr., W., Timoshenko, S. P., Young, D. H., 1990, *Vibration Problems in Engineering*, Wiley.

[30] Houbolt, J. C., and Brooks, G. W., 1957, "Differential Equations of Motion for Combined Flapwise Bending, Chordwise Bending, and Torsion of Twisted Nonuniform Rotor Blades," NACA Technical Note 3905, Langley Aeronautical Laboratory, Virginia.

